INORGANIC CHEMISTRY
FRONTIERS

RESEARCH ARTICLE

View Article Online
View Journal | View Issue

Cite this: *Inorg. Chem. Front.*, 2024, **11**, 3021

Vegard's law in multivariate libraries of porous interpenetrated zirconia organic frameworks†

Jacob I. Furst, ‡[a,b] Jacob T. Bryant, ‡[a,b] Kyle R. Langlois,[a,b] Shea D. Myers,[c] Azina Rahmani,[a,b] David C. Fairchild,[a,b] Rishabh Mehta,[a,b] Titel Jurca, *[a,b] Jason B. Benedict *[c] and Fernando J. Uribe-Romo *[a,b]

Received 6th February 2024,
Accepted 19th April 2024

DOI: 10.1039/d4qi00354c

rsc.li/frontiers-inorganic

In this contribution we demonstrate that metal–organic frameworks (MOFs) with suitable underlying topological structure are amenable for the preparation of MOF-based substitutional solid-solutions (SSS) that follow Vegard's law. Preparation of multivariate (MTV) libraries of Porous Interpenetrated Zirconia Organic Frameworks (PIZOF) using homeomorphic links of different length (18.6 and 19.3 Å) result in the formation of SSS that exhibit linearity between composition and structure. We prepared seven MTV MOF libraries (40 unique compositions) and observed relations in composition input/output ratio, composition/lattice parameter (Vegard's law), and between composition obtained from NMR and from PXRD. We further show that SSS formation has dependence on linker solubility, stability, and steric hindrance caused by the presence of functional groups. We demonstrate that solid-solution strategies can be utilized as part of the synthetic toolkit for the preperation of reticular crystals with desired composition, structure, and properties.

The ability to design stable multivariate metal–organic frameworks (MTV MOFs)[1] with targeted structure and composition requires for the crystal engineer to predict both structure and metrics based solely on the ratios and geometries of the molecular building blocks. This kind of control can be established by finding predictable relations between crystal structures and their compositions, as it is observed in inorganic substitutional solid solutions (SSS) that follow Vegard's law.[2] Vegard's law states that in sphere-packed solids, there are empirical relations between composition and crystal properties, *e.g.*, lattice parameters or cell volume.[3] The application of Vegard's law in inorganic SSS has enabled the preparation of many complex applied materials such as blue LEDs,[4] Cr-ruby lasers,[5] Li-ion batteries,[6] high entropy alloys,[7] and quantum dots.[8] In MOF synthesis, Vegard's law has been previously observed, but mostly to the mixing of metal ions.[9–19] From the point of view of the organic links, only a handful of examples have been presented.[20–28]

In this work, we demonstrate that Vegard's law is applicable to multivariate MOFs that have simple topological structures. For this, we utilize mixtures of homeomorphic links of different length and study the crystallographic traits of the prepared MOFs. Homeomorphisms in MOFs (Fig. 1a), refer to transformations that preserve the topological structure of the crystal (periodic net). Our hypothesis is that by varying the ratio of links in the form of A_xB_{1-x}, where A and B are homeomorphic links, should produce crystals with the relations expected in Vegard's law. Our approach consists of choosing a MOF system whose underlying topology is described by periodic nets that are *default* and *edge-1-transitive*.[29,30]

We selected Porous Interpenetrated Zirconia Organic Frameworks (PIZOF, Fig. 1b), a family of stable MOFs that bear the topology of the **fcu-c** net.[31–44] This net is a catenated form of **fcu**, the default net for cuboctahedral vertices.[45] The **fcu** net is edge-1-transitive,[46] it has a cubic space group symmetry in its maximum symmetry embedding, which provide for easy characterization of the lattice parameters *via* powder X-ray diffraction (PXRD) methods. The links used are linear and homeomorphic derivatives of oligo-phenylene and oligo-phenylene-ethynylene dicarboxylates. We selected **QPDC-Me** and **PEPEP-X** links (Fig. 1c) that contain heteroatom and solubilizing groups. The MOF made with **QPDC** (PIZOF-1) is the MOF matrix/solvent, and the **PEPEP** links are the solute (in PIZOF-2). The links have carboxylate-carboxylate distances of 18.6 and 19.3 Å respectively, corresponding to an average difference in length of 3.8%. We hypothesize that size differ-

[a]*Department of Chemistry, University of Central Florida College of Sciences, Orlando, Florida, USA. E-mail: Fernando@ucf.edu, Titel.Jurca@ucf.edu*
[b]*REACT: Renewable Energy and Chemical Transformations cluster, University of Central Florida, Orlando, FL 32814, USA*
[c]*Department of Chemistry, University at Buffalo, The State University of New York, Buffalo, NY 14260, USA. E-mail: Jbb6@buffalo.edu*
†Electronic supplementary information (ESI) available. See DOI: https://doi.org/10.1039/d4qi00354c
‡Equal contribution.

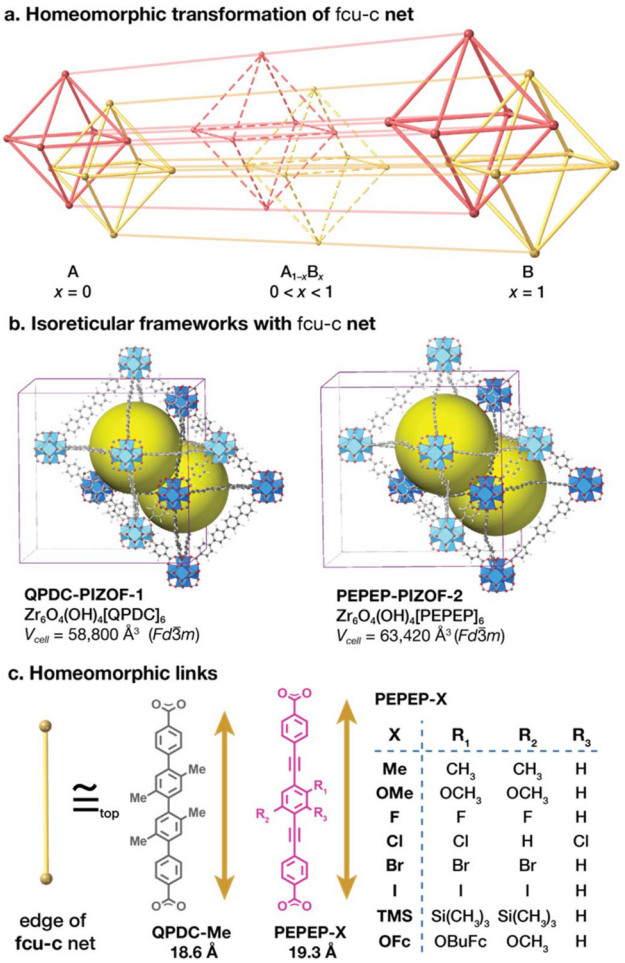

Fig. 1 (a) Graph representation of a homeomorphic transformation in the **fcu-c** net as function of edges A and B in the form A_xB_{1-x}. (b) Crystal structures of the pure-link PIZOF-1 and PIZOF-2 MOFs used in this study. Colour code: gray spheres = carbon, white = hydrogen, red = oxygen, blue polyhedra = Zr, yellow spheres = pores. Colour tones represent each interpenetrating framework. (c) Homeomorphic dicarboxylate links of varied length and heteroatom functionalization used in this study. Table indicates functional groups.

ences of <5% are favourable for SSS formation as it is for inorganic phases.[3] Furthermore, we probed the influence of functionalization of the solute links. To this end, PEPEP links were functionalized with heteroatom groups on the central ring (Fig. 1c) to probe SSS formation with respect to their internal structure.

We prepared seven MTV libraries and observed two kinds of behaviour: links that form complete MTV solid solutions and follow Vegard's law, and links that form partial MTV solid solutions that deviate from Vegard's law. We speculate that link-link steric hinderance is among the determining factors for solid solution formation. These libraries allowed us to validate our method for composition determination from non-destructive diffraction methods. Providing new strategies for the preparation of complex crystals with predetermined composition, metrics, and properties.

Results and discussion

We prepared MTV MOF libraries using standard MOF solvothermal crystallizations at 120 °C in glass reactors, by mixing $ZrCl_4$ and MTV links at specified input ratios in DMF/acetic acid/toluene mixtures (see ESI†). Our method produced both bulk microcrystalline powders and single crystals with compositions $Zr_6O_4(OH)_4[links]_6$, where the input composition of the links was varied in each library. Each library is a binary mixture of short and long links (**QPDC** and **PEPEP**, respectively, Fig. 1c) that have compositions with formula $Zr_6O_4(OH)_4[\mathbf{QPDC}_{1-x}\mathbf{PEPEP}_x]_6$, where x is the mol fraction of **PEPEP** links and $x \in [0,1]$. The input/output (I/O) compositions of these libraries were determined by ^{1}H NMR of digested samples, where we compared the ratio of the integrals for each monomer signal. The purpose of constructing I/O plots is to demonstrate control over the composition, *i.e.*, the relations between the target and the experimental ratios. Our aim is to achieve 1 : 1 I/O incorporation, which can be assessed by the slope of this plot. Once we determine the experimental output composition, we can construct Vegard's plots that relate the experimental parameters and compositions of the MOF.

The first library contains only methyl solubilizing groups on the central rings of the links. We observed a linear I/O composition slope of 1.0891 ± 0.0581 (Fig. 2a) in all the composition range, indicating that these links produce a complete solid solution. We also fitted a logistic function (eqn (S1)†) which typically accounts for interactions between the components of the mixture, observing good nonlinear fittings. We observe that both fittings are very close to each other suggesting **QPDC**/**PEPEP** link-link interactions that affect composition. The PXRD patterns of this library exhibits sharp diffraction lines (Fig. S18†), indicating high degree of crystallinity. The first and strongest diffraction line, the 111 peaks, exhibit a shift in peak position from 4.00 to 3.85 2θ-degrees (CuKα), indicating an expansion of the cell with increased **PEPEP-Me** content. This peak shift trend was also observed at higher angles, indicating a true change in lattice parameter, and not an instrumental artifact (like zero-shift). Indexing of both single crystals and powders provided cubic lattice parameters that are in good agreement with each other in triplicates, as well as with the expected values from the output composition following Vegard's law (Fig. 2b). The Vegard's plot indicates that there is a linear relation between the amount of **PEPEP-Me** and the lattice parameter. This is evidenced by the value of the correlation coefficient, R^2, the closer to 1 the more linear the correlation. In this library, powders and single crystals provide a coefficient of R^2 = 0.9871 and R^2 = 0.9695, respectively, indicating good linearity. All the prepared samples were porous, as exhibited in their N_2 gas isotherm (77 K), the only significant trend that we observed is that intermediate compositions, *e.g.* 50% and 60%, show higher uptakes, higher BET surface areas, higher pore volumes, and a higher frequency of larger pores (see section (S8)†). We speculate that SSS formation may induce nonlinear porosity trends that require a separate study.

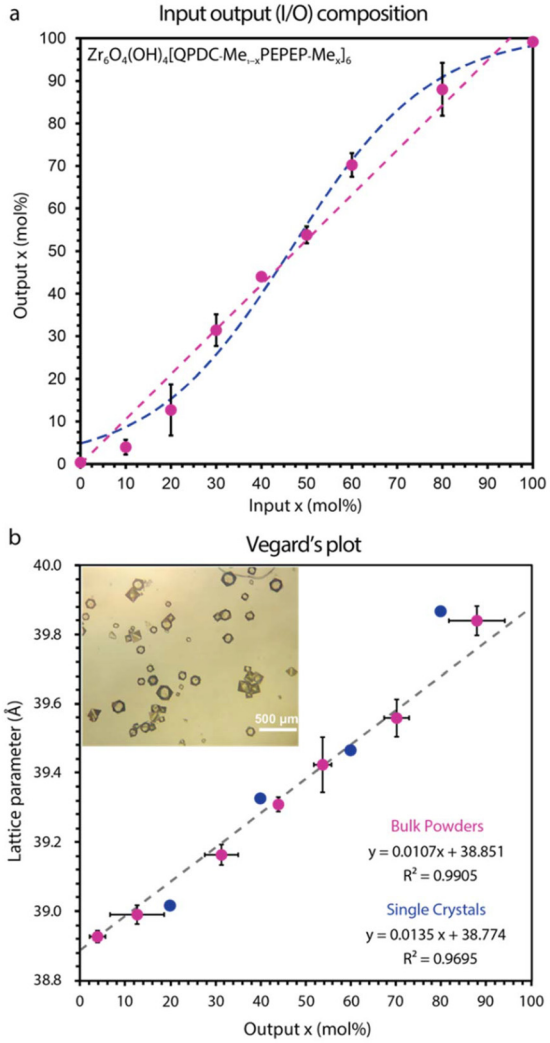

Fig. 2 (a) Input–output (I/O) composition plot of **QPDC-Me/PEPEP-Me** MTV library. Linear fitting is represented by the pink trace, and the logistic fitting is represented by the blue trace. (b) Vegard's plot of powder (pink) and single crystal (blue) **QPDC-Me/PEPEP-Me** MTV library. Linear fitting and R^2 for outputs *versus* lattice parameters are indicated. The ideal slope between 0% and 100% is in grey. Inset optical images of single crystals. Scale bar is indicated.

We then investigated the effect of functional group substitution on the central ring of the **PEPEP** link with respect to crystal formation and SSS behaviour. We prepared seven **PEPEP** links that contained heteroatom groups: methoxy (O), ω-alkylferrocene (Fe), fluoro (F), chloro (Cl), bromo (Br), iodo (I), and trimethylsilyl (Si). These links are also homeomorphic, regardless of having different associated chemistries (*e.g.* sterics and electronics), so they should exhibit SSS formation. The heteroatom solute links were prepared in a modular convergent fashion and were incorporated in libraries using similar synthesis strategies (see ESI†). The MTV libraries that successfully crystallize (Fig. 1c) exhibited two kinds of behaviours: Formation of complete solid solutions that follow Vegard's law, and formation of partial solid solutions with deviation from Vegard's law. Links **PEPEP-OMe**, **PEPEP-F**, and **PEPEP-Fc** form complete solid solutions with I/O slopes of 1.01 ± 0.07, 1.09 ± 0.13, and 1.07 ± 0.16 respectively (Fig. 3a), showing nearly linear trends *vs.* input composition. Both **PEPEP-F** and **PEPEP-Fc** deviate slightly from linearity at higher inputs, indicating that the links may be interacting during crystallization, as we previously observed when using acene links.[34] We fitted the I/O plots of these two libraries with logistic functions (see Fig. S8 and Fig. S13†). In contrast, when a MTV was made with links of the same size that contained **PEPEP-OMe** and **PEPEP-Fc** as matrix and solvent, respectively, we observed a more linear 1 : 1 input–output correlation (m =

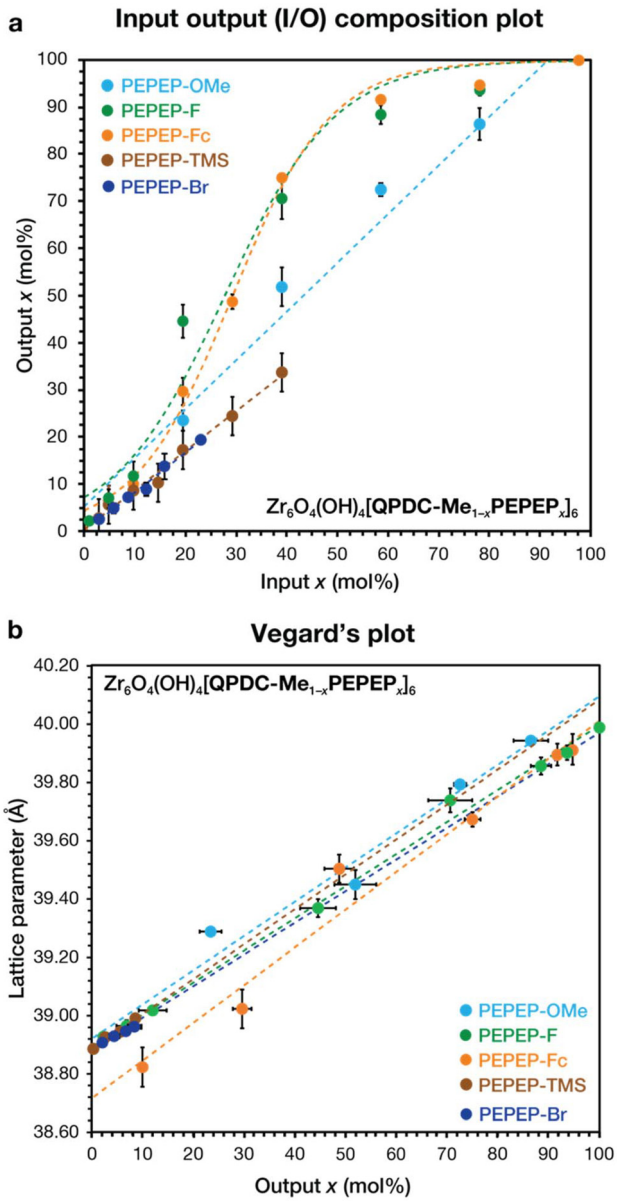

Fig. 3 (a) I/O plot, and (b) Vegard's plot of **QPDC-Me/PEPEP-X** MTV libraries that exhibit successful SSS formation. **PEPEP-OMe** = burgundy, **PEPEP-F** = **green**, **PEPEP-Fc** = orange, and **PEPEP-TMS** = brown, **PEPEP-Br** = dark blue. Error bars are from triplicate measurements.

0.9666, R^2 = 0.9968).[33] This Suggests that functionalization of the central ring plays a role in MTV library formation in conjunction with the differences in length. This effect was further accentuated when using sterically bulky substituents, like trimethylsilyl (TMS) in **PEPEP-TMS**. This **QPDC-Me**/**PEPEP-TMS** library exhibited crystal formation up to 40% input (see Fig. S21†), indicating a partial solid-solution with I/O slope of m = 0.8224 ± 0.0307 and R^2 = 0.9917. Interestingly, the Vegard's plot (Fig. S47†) shows linearity but only up to 10% output composition (R^2 = 0.9788), above this concentration the lattice parameter shrinks slightly before producing samples with large sample spread and lower indexing reliability. We believe these deviations in structure/composition are due to the appearance of defects caused by bulky TMS groups. The MTV system including **PEPEP-Br** showed similar results to the **PEPEP-TMS**. This library only crystallized up to 15%, and at higher input concentration the mother liquor turned deep red and does not form crystalline powders. The **QPDC-Me**/**PEPEP-Br** has a linear I/O slope of m = 0.8548 ± 0.0201. Similarly, the Vegard's plot (**S65**) also sees deviations from linearity at 10% input and above. EDS mapping of selected compositions (10% **PEPEP-TMS**, 80% **PEPEP-Fc**, and 90% **PEPEP-F**) observed even dispersion of heteroatoms in the mapped crystals. Further indicating mixing of the links as well as the lack of core–shell crystal formation.[47–49] In-depth crystallographic, gas adsorption, and electron microscopy studies are ongoing to elucidate these observations.

Some heteroatom containing links did not follow our hypothesis, exhibiting irregular MOF or MTV formation. **PEPEP** links with chlorines *ortho* to each other (**PEPEP-Cl**), exhibited limited solubility and thus unpredictable crystallization and SSS formation. Whereas the MOFs with 100% **PEPEP-Cl** crystallized successfully, SSS formation of the MTV was nonuniform, obtaining mixed phase samples of unpredictable composition and with recrystallized **PEPEP-Cl** link. This emphasizes the need for soluble links when preparing MTV MOFs. Also, we observed that **PEPEP-I** decomposes during MOF synthesis at all compositions and temperatures. This was evidenced by the mother liquor turning a deep purple during solvothermal synthesis similar to **PEPEP-Br**. Attempts to grow MTV crystals at lower temperatures and longer times were not successful Attemptsto prepare MTVs using terphenyl dicarboxylate (**TPDC**) and **QPDC-Me** as links with size difference of 21% (14.697 Å for **TPDC**) resulted in phase separation of PIZOF-1 and UiO-68 mixtures. Further studies will investigate size difference tolerance and SSS formation.

From Vegard's plots, we used the indexed lattice parameter (a_{indexed}) to solve for the composition according to the ideal trend between pure phases:

$$x_{\text{XRD}} = \frac{a_{\text{indexed}} - a_{\text{PIZOF-1}}}{a_{\text{PIZOF-2}} - a_{\text{PIZOF-1}}} \quad (1)$$

where x_{XRD} is the experimental composition from indexing, a_{indexed} is the indexed lattice parameter, $a_{\text{PIZOF-1}}$ and $a_{\text{PIZOF-2}}$ are the lattice parameters of the pure phases. We then plotted the experimental composition obtained from NMR *vs.* the experimental composition from indexed PXRDs of all samples. We found a global linear trend with a slope of m = 1.0215 ± 0.0201 and R^2 = 0.9653 for the **QPDC-Me**/**PEPEP-Me** system (Fig. 4a). This linear correlation falls very close to the ideal analytical parameters (m = 1, b = 0, R^2 = 1),[50] indicating that it is possible to determine MTV compositions from diffraction, as long as functional groups in the links are of sufficient steric bulk to allow SSS formation (*e.g.* up to 10 mol% in **PEPEP-TMS** and 7.5% in **PEPEP-Br**). This observation indicates that accurate composition of a sample can be obtained from non-destructive PXRD methods with accuracy. We believe that the demonstration of these linear relations in tailored crystals to be the foundation for the preparation of more complex MOF-based phases for applications that require high compositional and crystallographic precision.

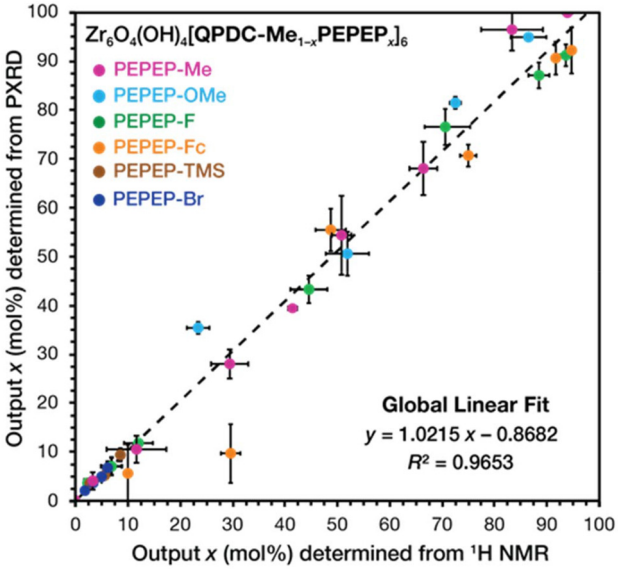

Fig. 4 Regression plot to compare composition obtained from NMR *vs.* composition obtained from PXRD with linear fitting and equation of **QPDC**/**PEPEP-X** MTV libraries. Note that all MTVs are complete solid-solutions except **PEPEP-TMS** and **PEPEP-Br**, which exhibit linearity up to 10 mol%.

Conclusions

We demonstrated that by choosing a MOF crystal with the precise topological features, it is possible to apply Vegard's law when using mixtures of homeomorphic links at varied ratios. For this, we successfully prepared seven libraries of MTV MOFs based on the PIZOF family of MOFs, observing linear trends between input and output link composition, between output composition and lattice parameters, and between composition from NMR spectroscopy and from PXRD indexing. We further explored the effect of functionalization of the central ring of the longer link, observing the SSS formation to be dependent on link-link interactions, particularly from steric hinderance. This work provides a synthesis approach for the

design of frameworks with complex compositions utilizing topology and crystallography as a guide, extending the applicability of Vegard's law from sphere-packed solids to molecular frameworks. Our strategy presents a toolbox that enables the design of MOF crystals with tunable topology, complex composition, and controlled lattice parameters that will further enable the design of even more complex MOFs towards direct applications. Future goals include to determine tolerance for size difference in links, explore the influence of defects, and the effects of the topology.

Author contributions

FJU, JIF, JTB, TJ conceived the project. JIF, JTB, KRL, DCF, AR and RM performed synthesis and characterization. SDM, JBB performed single crystal studies. FJU, JIF, JTB wrote manuscript.

Conflicts of interest

The authors declare no competing financial interests.

Acknowledgements

Financial support has been provided by the National Science Foundation awards no. DMR-2118201 (F. J. U.) and award no. DMR-2003932 (J. B. B.). Work at Argonne National Laboratory was supported by the U.S. Department of Energy (DOE), Office of Basic Energy Sciences, Division of Chemical Sciences, Geosciences, and Biosciences, Catalysis Science Program under contract no. DE-AC-02-06CH11357. We would like to thank Ms Taylor M. Currie and Mr Justin Arami for technical assistance.

References

1 H. Deng, C. J. Doonan, H. Furukawa, R. B. Ferreira, J. Towne, C. B. Knobler, B. Wang and O. M. Yaghi, Multiple Functional Groups of Varying Ratios in Metal-Organic Frameworks, *Science*, 2010, **327**, 846–850.
2 A. R. West, *Solid State Chemistry and its Applications. Chapter 10 Solid Solutions*, Wiley and Sons, Chichester, West Sussex, England, 1st edn, 1984.
3 A. R. Denton and N. W. Ashcroft, Vegard's law, *Phys. Rev. A*, 1991, **43**, 3161–3164.
4 S. N. Shuji Nakamura and T. M. Takashi Mukai, High-Quality InGaN Films Grown on GaN Films, *Jpn. J. Appl. Phys.*, 1992, **31**, L1457.
5 T. H. Maiman, Stimulated Optical Radiation in Ruby, *Nature*, 1960, **187**, 493–494.
6 J. T. Warner, in *Lithium-Ion Battery Chemistries*, ed. J. T. Warner, Elsevier, 2019, pp. 99–114. DOI: 10.1016/B978-0-12-814778-8.00005-3.
7 J. W. Yeh, S. K. Chen, S. J. Lin, J. Y. Gan, T. S. Chin, T. T. Shun, C. H. Tsau and S. Y. Chang, Nanostructured High-Entropy Alloys with Multiple Principal Elements: Novel Alloy Design Concepts and Outcomes, *Adv. Eng. Mater.*, 2004, **6**, 299–303.
8 R. W. Meulenberg, T. van Buuren, K. M. Hanif, T. M. Willey, G. F. Strouse and L. J. Terminello, Structure and Composition of Cu-Doped CdSe Nanocrystals Using Soft X-ray Absorption Spectroscopy, *Nano Lett.*, 2004, **4**, 2277–2285.
9 M. Lammert, C. Glißmann and N. Stock, Tuning the stability of bimetallic Ce(iv)/Zr(iv)-based MOFs with UiO-66 and MOF-808 structures, *Dalton Trans.*, 2017, **46**, 2425–2429.
10 O. Kozachuk, M. Meilikhov, K. Yusenko, A. Schneemann, B. Jee, A. V. Kuttatheyil, M. Bertmer, C. Sternemann, A. Pöppl and R. A. Fischer, A Solid-Solution Approach to Mixed-Metal Metal–Organic Frameworks – Detailed Characterization of Local Structures, Defects and Breathing Behaviour of Al/V Frameworks, *Eur. J. Inorg. Chem.*, 2013, **2013**, 4546–4557.
11 A. S. Munn, G. J. Clarkson, F. Millange, Y. Dumont and R. I. Walton, M(ii) (M = Mn, Co, Ni) variants of the MIL-53-type structure with pyridine-N-oxide as a co-ligand, *CrystEngComm*, 2013, **15**, 9679–9687.
12 J. Bitzer, S.-L. Heck and W. Kleist, Tailoring the breathing behavior of functionalized MIL-53(Al,M)-NH2 materials by using the mixed-metal concept, *Microporous Mesoporous Mater.*, 2020, **308**, 110329.
13 Y. Liu, D. Liu and C. Wang, Bivalent metal-based MIL-53 analogues: Synthesis, properties and application, *J. Solid State Chem.*, 2015, **223**, 84–94.
14 J. Panda, D. Singha, P. K. Panda, B. C. Tripathy and M. K. Rana, Experimental and DFT Study of Transition Metal Doping in a Zn-BDC MOF to Improve Electrical and Visible Light Absorption Properties, *J. Phys. Chem. C*, 2022, **126**, 12348–12360.
15 Y. Li, K. Pascal and X.-J. Jin, Ni–Mo modified metal–organic frameworks for high-performance supercapacitance and enzymeless H_2O_2 detection, *CrystEngComm*, 2020, **22**, 5145–5161.
16 A. Nowacka, P. Briantais, C. Prestipino and F. X. Llabrés I Xamena, Facile "Green" Aqueous Synthesis of Mono- and Bimetallic Trimesate Metal–Organic Frameworks, *Cryst. Growth Des.*, 2019, **19**, 4981–4989.
17 T. Devic, V. Wagner, N. Guillou, A. Vimont, M. Haouas, M. Pascolini, C. Serre, J. Marrot, M. Daturi, F. Taulelle and G. Férey, Synthesis and characterization of a series of porous lanthanide tricarboxylates, *Microporous Mesoporous Mater.*, 2011, **140**, 25–33.
18 T. Panda, S. Horike, K. Hagi, N. Ogiwara, K. Kadota, T. Itakura, M. Tsujimoto and S. Kitagawa, Mechanical Alloying of Metal–Organic Frameworks, *Angew. Chem., Int. Ed.*, 2017, **56**, 2413–2417.
19 P. R. Donnarumma, C. Copeman, M. Richezzi, J. Sardilli, H. M. Titi and A. J. Howarth, Deciphering Trends in Structural Parameters of RE-UiO-66 Metal–Organic

Frameworks through Single Crystal Analysis, *Cryst. Growth Des.*, 2024, **24**, 1619–1625.

20 R. L. Li, A. Yang, N. C. Flanders, M. T. Yeung, D. T. Sheppard and W. R. Dichtel, Two-Dimensional Covalent Organic Framework Solid Solutions, *J. Am. Chem. Soc.*, 2021, **143**, 7081–7087.

21 S. Yuan, L. Huang, Z. Huang, D. Sun, J.-S. Qin, L. Feng, J. Li, X. Zou, T. Cagin and H.-C. Zhou, Continuous Variation of Lattice Dimensions and Pore Sizes in Metal–Organic Frameworks, *J. Am. Chem. Soc.*, 2020, **142**, 4732–4738.

22 M. Li, D. Li, M. O'Keeffe and O. M. Yaghi, Topological Analysis of Metal–Organic Frameworks with Polytopic Linkers and/or Multiple Building Units and the Minimal Transitivity Principle, *Chem. Rev.*, 2014, **114**, 1343–1370.

23 J. Bitzer, A. Titze-Alonso, A. Roshdy and W. Kleist, The introduction of functional side groups and the application of the mixed-linker concept in divalent MIL-53(Ni) materials, *Dalton Trans.*, 2020, **49**, 9148–9154.

24 M. Wang, T. Zeng, Y. Yu, X. Wang, Y. Zhao, H. Xi and Y.-B. Zhang, Flexibility On-Demand: Multivariate 3D Covalent Organic Frameworks, *J. Am. Chem. Soc.*, 2024, **146**, 1035–1041.

25 L. Feng, S. Yuan, J.-S. Qin, Y. Wang, A. Kirchon, D. Qiu, L. Cheng, S. T. Madrahimov and H.-C. Zhou, Lattice Expansion and Contraction in Metal-Organic Frameworks by Sequential Linker Reinstallation, *Matter*, 2019, **1**, 156–167.

26 Y. Hu, X. Zhang, R. S. H. Khoo, C. Fiankor, X. Zhang and J. Zhang, Stepwise Assembly of Quinary Multivariate Metal–Organic Frameworks via Diversified Linker Exchange and Installation, *J. Am. Chem. Soc.*, 2023, **145**, 13929–13937.

27 Z. Lu, H. Tan, H. Lin, X. Cai, L. Du and Q. Liu, Stepwise Node-Locking of a Mesoporous Zirconium Metal–Organic Framework Toward Enhanced Cycle Stability for Water Adsorption, *Chem. Mater.*, 2024, **36**, 2652–2660.

28 G. Valente, P. Ferreira, M. A. Hernández-Rodríguez, C. D. S. Brites, J. S. Amaral, P. Zelenovskii, F. A. A. Paz, S. Guieu, J. Rocha and M. Souto, Exploring the Luminescence, Redox, and Magnetic Properties in a Multivariate Metal–Organic Radical Framework, *Chem. Mater.*, 2024, **36**, 1333–1341.

29 O. M. Yaghi, M. O'Keeffe, N. W. Ockwig, H. K. Chae, M. Eddaoudi and J. Kim, Reticular synthesis and the design of new materials, *Nature*, 2003, **423**, 705–714.

30 H. Jiang, D. Alezi and M. Eddaoudi, A reticular chemistry guide for the design of periodic solids, *Nat. Rev. Mater.*, 2021, **6**, 466–487.

31 A. Schaate, P. Roy, T. Preuße, S. J. Lohmeier, A. Godt and P. Behrens, Porous Interpenetrated Zirconium–Organic Frameworks (PIZOFs): A Chemically Versatile Family of Metal–Organic Frameworks, *Chem. – Eur. J.*, 2011, **17**, 9320–9325.

32 J. Lippke, B. Brosent, T. von Zons, E. Virmani, S. Lilienthal, T. Preuße, M. Hülsmann, A. M. Schneider, S. Wuttke, P. Behrens and A. Godt, Expanding the Group of Porous Interpenetrated Zr-Organic Frameworks (PIZOFs) with Linkers of Different Lengths, *Inorg. Chem.*, 2017, **56**, 748–761.

33 G. S. Mohammad-Pour, K. O. Hatfield, D. C. Fairchild, K. Hernandez-Burgos, J. Rodríguez-López and F. J. Uribe-Romo, A Solid-Solution Approach for Redox Active Metal–Organic Frameworks with Tunable Redox Conductivity, *J. Am. Chem. Soc.*, 2019, **141**, 19978–19982.

34 W. J. Newsome, A. Chakraborty, R. T. Ly, G. S. Pour, D. C. Fairchild, A. J. Morris and F. J. Uribe-Romo, J-dimer emission in interwoven metal–organic frameworks, *Chem. Sci.*, 2020, **11**, 4391–4396.

35 A. Torres-Huerta, D. Galicia-Badillo, A. Aguilar-Granda, J. T. Bryant, F. J. Uribe-Romo and B. Rodríguez-Molina, Multiple rotational rates in a guest-loaded, amphidynamic zirconia metal–organic framework, *Chem. Sci.*, 2020, **11**, 11579–11583.

36 E. Virmani, J. M. Rotter, A. Mähringer, T. von Zons, A. Godt, T. Bein, S. Wuttke and D. D. Medina, On-Surface Synthesis of Highly Oriented Thin Metal–Organic Framework Films through Vapor-Assisted Conversion, *J. Am. Chem. Soc.*, 2018, **140**, 4812–4819.

37 P. Roy, A. Schaate, P. Behrens and A. Godt, Post-Synthetic Modification of Zr-Metal–Organic Frameworks through Cycloaddition Reactions, *Chem. – Eur. J.*, 2012, **18**, 6979–6985.

38 T. von Zons, L. Brokmann, J. Lippke, T. Preuße, M. Hülsmann, A. Schaate, P. Behrens and A. Godt, Postsynthetic Modification of Metal–Organic Frameworks through Nitrile Oxide–Alkyne Cycloaddition, *Inorg. Chem.*, 2018, **57**, 3348–3359.

39 R. Babarao, C. J. Coghlan, D. Rankine, W. M. Bloch, G. K. Gransbury, H. Sato, S. Kitagawa, C. J. Sumby, M. R. Hill and C. J. Doonan, Does Functionalisation Enhance CO2 Uptake in Interpenetrated Mofs? An Examination of the Irmof-9 Series, *Chem. Commun.*, 2014, **50**, 3238.

40 R. J. Marshall, Y. Kalinovskyy, S. L. Griffin, C. Wilson, B. A. Blight and R. S. Forgan, Functional Versatility of a Series of Zr Metal–Organic Frameworks Probed by Solid-State Photoluminescence Spectroscopy, *J. Am. Chem. Soc.*, 2017, **139**, 6253–6260.

41 A. T. Castner, H. Su, E. Svensson Grape, A. K. Inge, B. A. Johnson, M. S. G. Ahlquist and S. Ott, Microscopic Insights into Cation-Coupled Electron Hopping Transport in a Metal–Organic Framework, *J. Am. Chem. Soc.*, 2022, **144**, 5910–5920.

42 Z. Liu, Y. Wang and M. A. Garcia-Garibay, Rotational Dynamics of an Amphidynamic Zirconium Metal–Organic Framework Determined by Dielectric Spectroscopy, *J. Phys. Chem. Lett.*, 2021, **12**, 5644–5648.

43 W. J. Newsome, S. Ayad, J. Cordova, E. W. Reinheimer, A. D. Campiglia, J. K. Harper, K. Hanson and F. J. Uribe-Romo, Solid State Multicolor Emission in Substitutional Solid Solutions of Metal–Organic Frameworks, *J. Am. Chem. Soc.*, 2019, **141**, 11298–11303.

44 A. H. Assen, K. Adil, K. E. Cordova and Y. Belmabkhout, The chemistry of metal–organic frameworks with face-centered cubic topology, *Coord. Chem. Rev.*, 2022, **468**, 214644.
45 C. Bonneau and M. O'Keeffe, High-symmetry embeddings of interpenetrating periodic nets. Essential rings and patterns of catenation, *Acta Crystallogr., Sect. A: Found. Adv.*, 2015, **71**, 82–91.
46 M. O'Keeffe, Nets, tiles, and metal-organic frameworks, *APL Mater.*, 2014, **2**, 124106.
47 B. Lerma-Berlanga, C. R. Ganivet, N. Almora-Barrios, S. Tatay, Y. Peng, J. Albero, O. Fabelo, J. González-Platas, H. García, N. M. Padial and C. Martí-Gastaldo, Effect of Linker Distribution in the Photocatalytic Activity of Multivariate Mesoporous Crystals, *J. Am. Chem. Soc.*, 2021, **143**, 1798–1806.
48 A. Centrone, B. Lerma-Berlanga, A. J. Biacchi, C. Fernández-Conde, G. Pavlidis and C. Marti-Gastaldo, Direct Visualization of Chemically Resolved Multilayered Domains in Mixed-Linker Metal–Organic Frameworks, *Adv. Funct. Mater.*, 2023, **33**, 2302357.
49 O. Kwon, J. Y. Kim, S. Park, J. H. Lee, J. Ha, H. Park, H. R. Moon and J. Kim, Computer-aided discovery of connected metal-organic frameworks, *Nat. Commun.*, 2019, **10**, 3620.
50 J. N. Miller and J. C. Miller, Calibration methods in instrumental analysis, *Statistics and chemometrics for analytical chemistry*, Prentice Hall, Harlow, England, 4th edn, 2000, pp. 126–130.